nagra.

Arbeitsbericht NAB 22-19

Advanced Methodology for Activation Characterization (AMAC)

December 2022

National Cooperative
for the Disposal of
Radioactive Waste

Hardstrasse 73
P.O. Box
5430 Wettingen
Switzerland
Tel. +41 56 437 11 11

www.nagra.ch

nagra.

Arbeitsbericht NAB 22-19

Advanced Methodology for Activation Characterization (AMAC)

December 2022

KEYWORDS

Abfallvolumen, Activation, Aktivierung, Aktivierungsverteilung, AMAC, Decommissioning Waste, MCNP, MIRAM, MIRAM-RBG, RBG-Dokumentation

National Cooperative
for the Disposal of
Radioactive Waste

Hardstrasse 73
P.O. Box
5430 Wettingen
Switzerland
Tel. +41 56 437 11 11

www.nagra.ch

Nagra Arbeitsberichte ("Working Reports") present the results of work in progress that have not necessarily been subject to a comprehensive review. They are intended to provide rapid dissemination of current information.

NAB 22-19, December 2022: Corrigendum
This report was corrected for formatting and typographical errors in January 2023.

Table of Contents

List of Figures

List of Acronyms

ADVANTG	Automated Variance Reduction Generator
AGT	Waste Package Type
ALGOPACK	Algorithm-Optimized Packaging
AMAC	Advanced Methodology for Activation Characterization
API	Application Programming Interface
BWR	Boiling Water Reactor
ELB	Disposal Canister
ENDF	Evaluated Nuclear Data File
FA	Fuel Assembly
HDF5	Hierarchical Data Format 5
KKB	Beznau Nuclear Power Plant
KKG	Gösgen Nuclear Power Plant
KKL	Leibstadt Nuclear Power Plant
KKM	Mühleberg Nuclear Power Plant
KS	Cost Study
MCNP	Monte Carlo N-Particle (Transport Code)
MIRAM	Model Inventory for Radioactive Materials
NAB	Nagra Work Report
NEA	Nuclear Energy Agency
NPP	Nuclear Power Plant
NTB	Nagra Technical Report
ORNL	Oak Ridge National Laboratory
PWR	Pressurized Water Reactor
RBG	General License Application
RPV	Reactor Pressure Vessel
RSICC	Radiation Safety Information Computational Center
SCALE	Standardized Computer Analyses Licensing Evaluation
StSV	Radiological Protection Ordinance
VR	Variance Reduction
WW	Weight Window
WWG	Weight Window Generator

1 Introduction

A detailed understanding of the activity distribution within the nuclear power plant (NPP) at time of shutdown is essential for the planning of the decommissioning process and the corresponding segmentation strategy, choice of waste containers, packaging concepts, and logistics considerations.

Apart from the spent fuel present on the site, the radiological condition of the site is a result of two pathways: neutron activation and contamination. With almost 10^{17} neutrons released per second per MW (of thermal power), despite the many layers of shielding, a fraction of them successfully leaks out of the core, and eventually the reactor pressure vessel (RPV). These neutrons then interact with the nuclei in the surrounding materials (including their impurities). Most of the products created in these neutron reactions are radioactive. This process is referred to as neutron activation. Contamination results from direct contact with radioactive substances, generally within the primary loop.

Neutron activation is analyzed using neutron transport codes, which simulate the transport of neutrons from the core to all surrounding structures with which the neutrons interact. Contamination is generally determined through direct measurements. This report aims to provide an overview of the methodology employed by Nagra to quantify neutron activation in NPPs.

Nagra regularly updates its studies for the radiological characterization of all Swiss NPPs. Such efforts include the estimation of radioactivity in the NPP through neutron activation and radioactive contamination of structures and components within the controlled area of the reactor facility. To support these efforts, Nagra has developed an NPP activation analysis methodology, based on three-dimensional models of NPPs created for the particle transport code MCNP (Werner 2017).

The first uses of MCNP to characterize neutron activation in NPPs at Nagra (Volmert & Pantelias Garcés 2011a, Volmert & Pantelias Garcés 2011b, Volmert & Pantelias Garcés 2011c, Volmert & Pantelias Garcés 2011d) were performed in support of cost study 2011 (KS11) and MIRAM14 (Nagra 2014). The methodology was further developed in two PhD projects: the first (Pantelias Garcés 2013) focusing on the application of variance reduction to facilitate a higher level of model complexity and the second (Bykov 2019) developing a sequence to automate the activation calculations and manage the large quantities of data that the detailed calculations produced. Following these developments, the methodology was named AMAC – Advanced Methodology for Activation Characterization. A scheme summarizing AMAC can be seen in Fig. 1-1.

AMAC is a versatile methodology, which can be applied to any nuclear reactor type and in support of different types of analyses:

- develop and optimize segmentation strategies and the associated packaging concepts for reactor internals and the RPV
- quantify the volume of activated concrete surrounding the RPV and how it changes for different disposal scenarios (e.g., after additional decay time)
- determine the activation depth of these structures to support the static investigations of the reactor building (answering whether the activated material can be safely removed while still preserving the structural integrity of the building)
- support calculations of the gamma dose rate resulting from the activation of the components and structures
- and describe the full nuclide vectors (originating from neutron activation) in all the different sections of the controlled zone

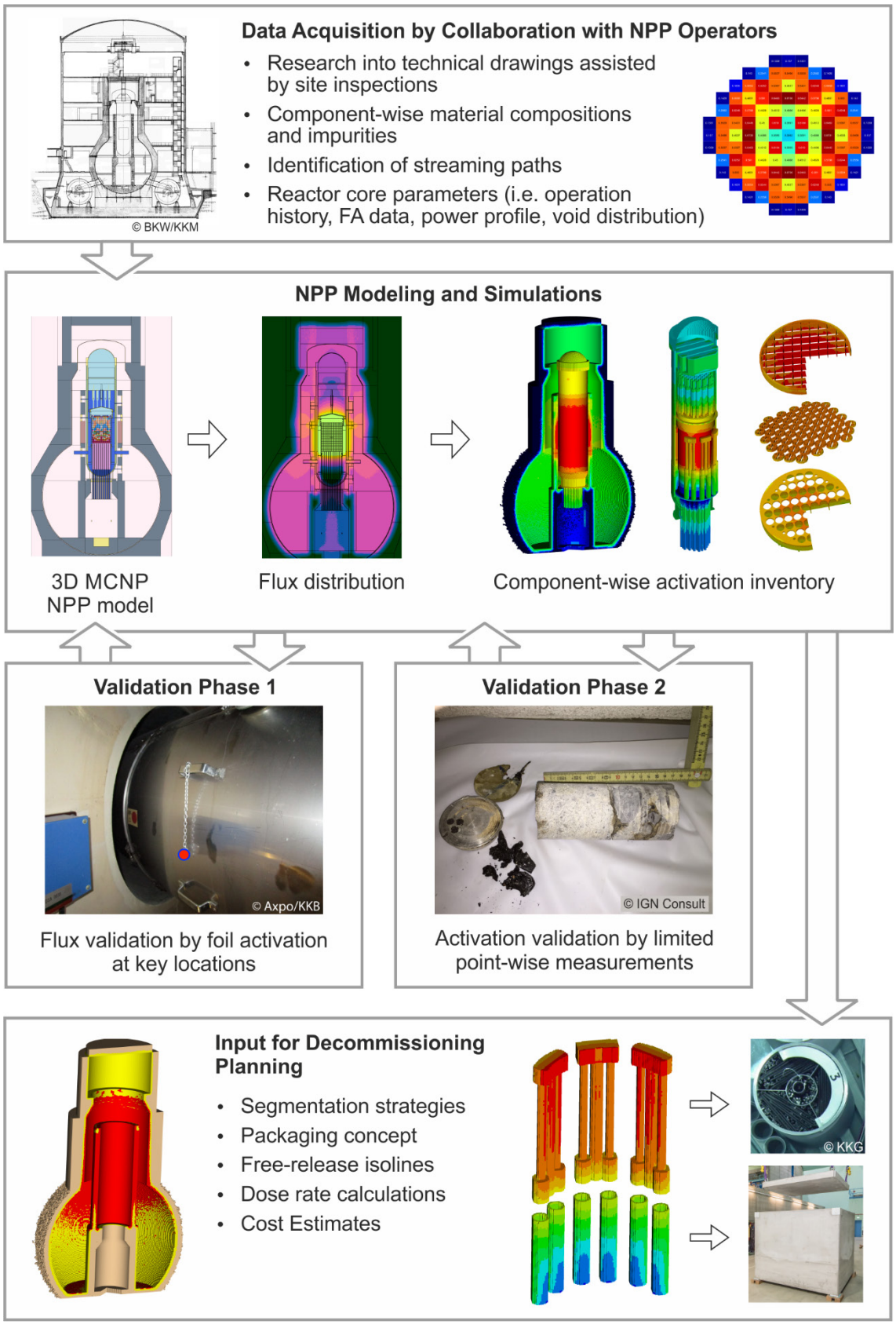

Fig. 1-1: Summary of AMAC (Advanced Methodology for Activation Characterization)

It should be noted that each of these applications has its own requirements on, for example, the target level of model detail. Typically, the ultimate goal of the AMAC model designer is to prepare an NPP model that can be used for *all* of these applications, or at least all that are envisioned for the NPP in question.

This report primarily aims to define AMAC as a methodology, specifying the individual steps and the software tools used. Additionally, this report details the application of AMAC in support of MIRAM (Model Inventory for Radioactive Materials) – the Nagra database of current and future waste used for long-term safety analyses of the deep geological repository. Specifically, how AMAC is used to characterize the nuclide inventories associated with MIRAM waste package types (*Abfallgebindetypen* – AGT) for the general license application (*Rahmenbewilligungs-gesuch* – RBG) version of MIRAM – MIRAM-RBG (Nagra 2023).

The structure of this report follows the individual steps of the scheme summarizing AMAC shown in Fig. 1-1. Chapter 2 describes the data acquisition process, the type of data that is collected, and the steps taken when the NPP cannot provide this data. The way this data is then used to build the MCNP models is explained in Chapter 3, with Chapter 4 discussing the types of calculations carried out. Chapter 5 explains the variance reduction techniques (as developed in (Pantelias Garcés 2013)) applied to these calculations to increase their computational efficiency. The calculation sequence for the activation calculations (as developed in (Bykov 2019)) is described in Chapter 6. The efforts undertaken to validate these MCNP models are discussed in Chapter 7. In order to deal with the large amount of results data produced by AMAC, various data management and analytics tools have been developed (AMAC Data Tools). These are documented in Chapter 8. The usage of these tools to describe a packaging concept for internals and RPV, as well as to characterize the activated sections of the surrounding structures, is explained in Chapters 9 and 10, respectively.

2 Data acquisition

In order to construct the MCNP model of the plant at the desired level of detail, technical drawings – detailing the geometry of the components and buildings – are provided by the plant. These are assisted by site visits, conversations with corresponding NPP experts, photographing the reactor building compartments, as well as by comparisons with technical documentation from other (similar) plants.

Accurate simulations of radiation transport require realistic definitions of material compositions and densities. Furthermore, activation calculations require detailed knowledge of material impurities. The material information consists of base material description (e.g., "stainless steel 304"), its density, and an impurity vector. Ideally, the latter would come from a chemical analysis of material samples taken from each component. However, in many cases no analysis results are available. Given this situation, AMAC uses the following sources of material description (in decreasing order of accuracy and therefore preference):

- direct chemical measurements
- measurements done in analogue NPPs for the same material
- impurity measurements for other, but similar, materials (e.g., impurities detected in RPV steel approximated using impurities in carbon steel found in rebar, and vice versa)
- literature values – particularly from (Evans et al. 1984), which provides an overview of numerous measurements from components of decommissioned US NPPs, but also from general material definitions (McConn et al. 2011) and standards (DIN 2013)

As an example of the direct chemical measurements of the modeled material, Fig. 2-1 shows a drill core extracted in 2017 from the containment building of KKB Unit 2. It was subsequently analyzed to evaluate the concentrations of lithium, boron, iron, cobalt, europium, thorium, and uranium impurities. The remaining impurities for KKB concrete were based on chemical analysis of KKL concrete, as well as literature values.

Core parameters used for the modeling are: NPP operating history and future forecast, fuel assembly (FA) geometrical and material description, nodal power distribution (captured at a representative point in time), and for boiling water reactors (BWR) the nodal void distribution. This information is typically provided directly by the NPP's core modeling group for a representative point during a typical cycle.

Fig. 2-1: Drill core extracted from the containment building of KKB Unit 2
Pisano (2018)

3 Modeling

Based on the geometrical, material, and core parameter information from Chapter 2, a three-dimensional MCNP model of the NPP is built.

While it's possible to have a high level of geometric detail throughout the NPP model, this is normally not the optimal approach. For components located close to the active core (internals, RPV) it's very desirable to model them in detail, since this increases the accuracy (and the level of detail) of the final activation distribution result. However, rooms or areas situated far away from the core (such as the drywell in KKM) are often occupied with machinery and other objects, which are installed, relocated, and removed, sometimes multiple times, during the lifetime of the plant. These changes are difficult to track and are thus almost never documented, making it impossible to accurately capture the shielding resulting from these objects. Instead, a conservative assumption is made assuming that all these rooms are empty. This results in the underestimation of the shielding and therefore overestimation of the flux. The extent of this overestimation grows with distance from the core (as more distance is traveled by neutrons through the empty rooms). As such, when modeling these areas, mainly only the general shape of the surrounding (or intersecting) walls must be captured. Overall, the resulting MNCP models visually appear to be very detailed near the core, with the degree of detail decreasing with the increasing distance from the core. An example can be seen in Fig. 4-1, showing the MCNP model of KKM. On the other hand, gaps and openings serve as streaming paths for neutrons and therefore need to be modeled in the maximum possible degree of detail, in order to accurately capture neutron transport through these areas. That is, all geometry relevant for the neutron streaming and transport is modeled in detail, regardless of the distance from the active core.

Reinforced concrete is generally treated as a mixture of concrete and steel rebar, where the rebar is assumed to occupy 5 vol% (unless more detailed information is available). For transport calculations, the concrete and steel rebar are homogenized together and treated as a mixture. Conversely, for the purposes of activation calculations, these two components are considered separately. To calculate the individual activation both materials are assumed to cover the same volume as the reinforced concrete mixture, with density adjusted to preserve the real material balance – that is, partial densities are used instead of the real material densities. This results in nuclide vectors representative of the real mass of each of the two present materials. This is particularly important for the purpose of clearance measurements, since it is currently assumed that for NPP decommissioning rebar is not separated from the concrete. That is, if the rebar steel is activated above the clearance limits, the particular segment of reinforced concrete cannot be released, regardless of how low the activity of the concrete itself might be.

With the reactor internals modeled explicitly and with an increased degree of detail, it is necessary to also improve the modeling of the active core. As was explored in (Scolaro 2016), both the real core shape and the accurate power profile have a strong impact on the total flux at the core boundary. This effect has a particularly significant impact on nearby components. As such, accurate modeling of the core shape and power distribution is paramount.

The core information provided by the NPP uses a nodal resolution of the core. The FAs are divided into a number of axial segments, with individual nodes representing one segment each. The total number of nodes used to express the active core is thus equal to the number of fuel assemblies (e.g., 240 for KKM) multiplied by the number of axial segments (e.g., 25 for KKM, resulting in 6'000 nodes in total). Each node has its own power value (used as MCNP particle emission probability), which exactly matches the provided data, and a material card, representative of its FA type, coolant density, and (for BWRs) void fraction.

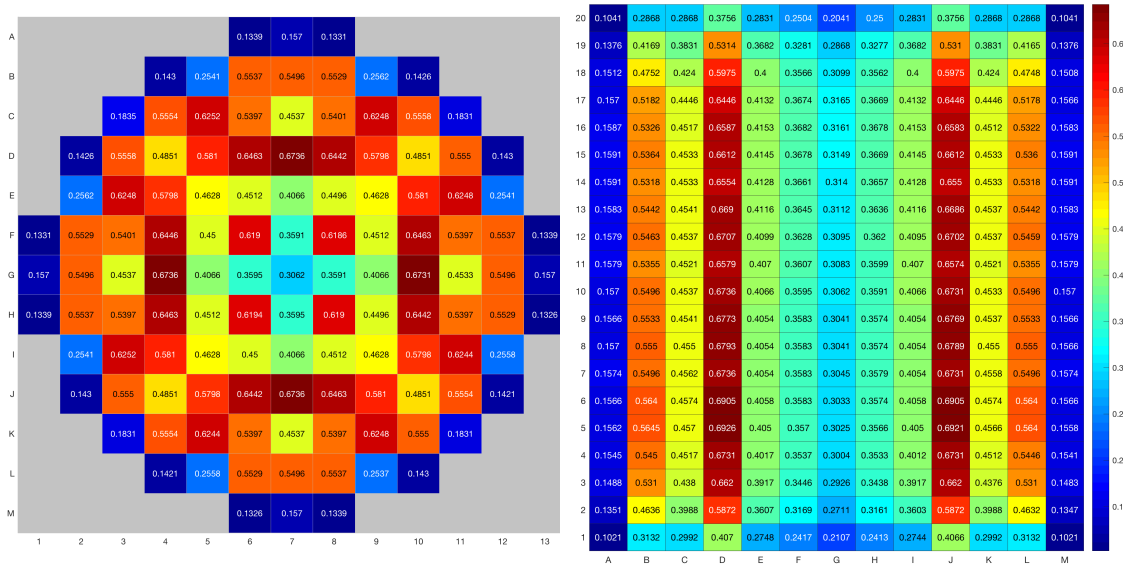

Fig. 3-1: Active core power distribution (relative probability of neutron emission) in the KKB MCNP model

Pisano (2018)

An example of the nodal structure of the active core in the MNCP model can be seen in Fig. 3-1, showing the active core from the KKB MCNP model. The pseudocolor represents the relative probability of neutron emission from the given node. These values are directly used in the MCNP source definition (the *SDEF* card) as MCNP cell probabilities.

Due to the MCNP lattice syntax, the input lines for the source term quickly become very long and complex. For this reason, an automated script has been developed, significantly reducing the engineering work necessary for creating the core model. As an input, the script user provides the core shape, the nodal void fraction data, the nodal power data, and the geometrical details of a reference FA type (i.e., the most common in the core). The latter includes the number of fuel pins, water rods, and partial length fuel rods, as well as the diameter of the pellet, gap and cladding, and the dimensions of the FA box (if applicable). In reality, the burnup varies strongly between assemblies, with the distribution in the core being highly heterogeneous. However, as was explored in (Pantelias Garcés 2013) when the model is run in source-term mode and criticality is disabled (using the MCNP *NONU* card), the neutron leakage from the core is relatively insensitive to the burnup level of the fuel. This is because with fission reactions disabled, all neutron removal reactions are treated as neutron absorption (that is, the fission cross section is assimilated into the absorption cross section). As such, the depletion of fissile nuclides is approximately counter-balanced by the buildup of the fission products (Pantelias Garcés 2013). For this reason, for the purposes of these calculations, the same fuel composition is used for all fuel rods in all fuel assemblies in the core. For consistency, the composition was chosen to be representative of the (high burnup) assemblies in the outermost parts of the core, which are responsible for the majority of the radial neutron leakage. With fuel composition and the lattice taken as constant for all fuel assemblies, the overall (homogenized) material composition of each node is only a function of the (coolant) void fraction. That is, other than the void fraction, all other parameters remain constant.

Using the received information, the script performs a volume balance and obtains the nodal density for each node. While the lattice materials are always the same, the void fraction changes across the nodes, causing the density to vary. At this point, the script user has the freedom to

decide the number of MCNP material cards to be automatically generated by the script. Each node will then be assigned the MCNP material which most closely matches its homogenized material composition. It's therefore necessary to choose a sufficient number of MCNP materials, in order to accurately capture the variation of the nodal density (caused only by the variations in the void fraction).

In certain BWR FAs, some fuel rods are shorter than the others. Most commonly (in Switzerland), the partial length rods are divided between one-third length and two-thirds length rods, though some FAs instead have 56% length rods. It's desirable to capture the presence of these rods when defining the core material cards. For this purpose, the core script allows the user to split the active core into two parts, with top and bottom parts each getting their own set of separate material cards. This functionality allows the user to account for the partial length rods, albeit for only one partial-length rod length.

Each element of the MCNP lattice is then assigned a corresponding material card and its own nodal power value, reproducing the nodal power profile exactly matching the provided data.

Finally, the script automatically generates the MCNP input necessary to model this complex source term, ready to be pasted into the MCNP input file. As such, it's possible to test different core configurations with minimal effort and engineering time investment.

4 Neutron flux calculations

Once the MCNP model is completed, the neutron flux distribution in the system is calculated and analyzed. Several different calculations are performed within this step.

Analyzing the whole system, a mesh tally overlaying the whole geometry (or a two-dimensional slice of the whole geometry) is used to calculate either the total neutron flux, or its breakdown into the thermal (energy below 0.5 eV), epi-thermal (energy between 0.5 eV and 100 keV), and fast energy range (energy above 100 keV).

In general, as governed by the relevant cross sections, fast and thermal neutrons both exhibit characteristic behaviors. Fast neutrons travel long distances between individual interactions (as low cross sections lead to long mean free paths) and spread throughout the geometry in a beam-like fashion (i.e., the travelled paths are long straight lines). Thermal neutrons, on the other hand, undergo a lot of scattering interactions (with short mean free paths, caused by the large cross sections), which redirect their path. Consequently, thermal neutrons spread in a gas-like fashion. These behaviors have been explored for example in (Tamaseviciute 2011).

An example of this can be seen in Fig. 4-1, showing the distribution of the total neutron flux in KKM. Note that the range covered by the pseudocolor scale has been selected to showcase the important behavior of the flux distribution. That is, the flux is "cropped," with all values above 1e10 $n \cdot cm^{-2} \cdot s^{-1}$ shown in a single (bright yellow) color (up to the maximum value, located in the central region of the active core) and all values below 1e1 $n \cdot cm^{-2} \cdot s^{-1}$ also shown in the same (dark green) color.

These calculations provide a global overview of the neutron transport pattern and the first rough estimate of the expected neutron activation levels – though of course the actual extent of neutron activation depends also on the shape (that is, the energy distribution) of the neutron flux at the given location.

Further neutron transport studies are carried out in regions where neutron streaming is expected (or hinted at by the global flux maps). These calculations would use a finer mesh than the aforementioned whole system calculations. Their goal is to ensure that the observed neutron streaming paths match expectations and that all important openings and structures (as defined by the observation of the results) are modeled with sufficient level of detail.

The same MCNP calculation that calculates the total flux in the whole system can also be used to calculate the reaction rate of the Co-59 and Eu-151 (n,g) reactions, which can be used to calculate the global concentrations of Co-60 and Eu-152 – either per concentration of impurity (e.g., per 1 ppm) or assuming the impurity concentration of a particular material (such as stainless steel). If the impurity concentration of stainless steel is assumed for this calculation, the result would indicate the Co-60 concentration (and therefore specific activity) within stainless steel had it been present at the given location (even if it's not actually there). The detailed description of the procedure, including the incorporation of the NPP-specific operating history, can be found in (Scolaro 2016).

These results provide a useful overview over the specific activities to be expected in the different sections of the model, but due to the size and complexity of the model geometry, it's desirable to carry out a more detailed activation calculation on a per-component basis. That is, these results are used to identify activated components to be analyzed in more detail, as well as to determine the optimum target spatial resolution. Components, in which a strong gradient of activities is expected, are investigated with a finer mesh (to better capture the aforementioned gradients), while components with relatively homogeneous activity distribution are investigated with a relatively coarse mesh.

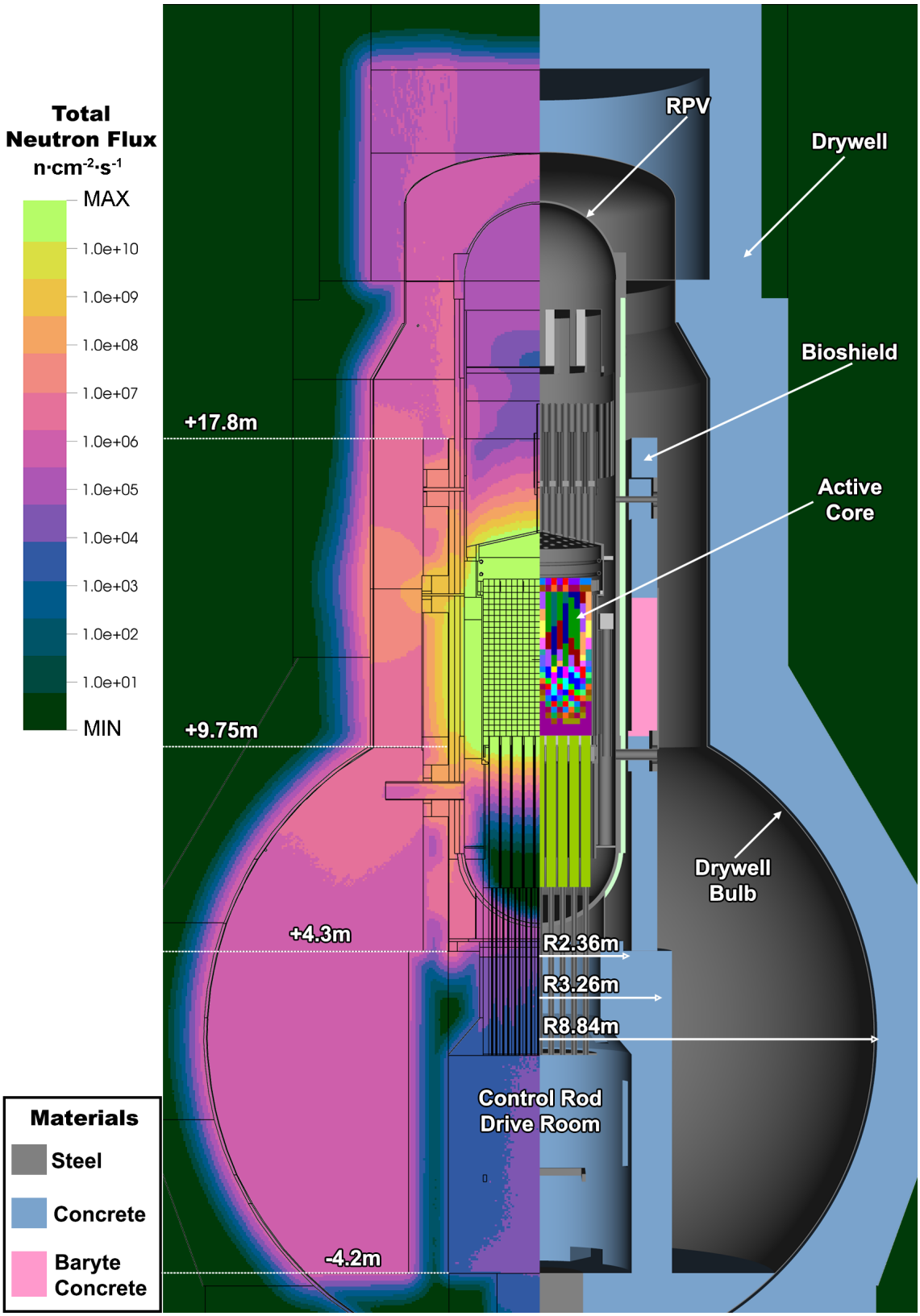

Fig. 4-1: MCNP model of KKM and the calculated total neutron flux distribution

Once the target level of detail is known for all components, mesh tallies are defined. Generally, each one component is covered by a single mesh tally. Components located very close to each other or even occupying the same general space (as the BWR lower core plate and the fuel assembly feet that fit into its openings) are sometimes jointly covered by a single mesh tally. Large components with very large activity gradients – such as the core shroud in BWRs or core barrel in PWRs – are typically split into a number of sub-components for computational efficiency reasons. Typically, the cell size in these mesh tallies is in the order of $5 \times 5 \times 5$ cm^3, but in some cases may be as small as $1 \times 1 \times 5$ cm^3. The energy bins used for these mesh tallies follow the SCALE-56 energy group structure (Wieselquist et al. 2020).

The code sequence making up AMAC is energy group structure agnostic – that is, *any* energy group structure can be used. As such, this is a user choice. A finer energy group structure provides more detail but increases the computational cost of statistical convergence. Various investigations were performed on this subject in (Bykov 2014), and during the work performed in (Bykov 2019), the SCALE-56 energy group structure was selected for the MIRAM-RBG work, as it captures the neutron flux with sufficient level of detail (for flux shapes typical for areas of interest for neutron activation calculations) and keeps the computational cost reasonable.

In order to obtain a converged result for all mesh tallies in a reasonable amount of time, variance reduction is needed. This is described in Chapter 5. Once obtained, the tally results serve as an input for the activation calculation sequence, described in Chapter 6.

Neutron transport calculations are carried out with a Monte Carlo particle transport code MCNP6, version 2.0 (also referred to as MCNP 6.2) (Werner 2017), using the ENDF/B-VII.1 cross section library (Chadwick et al. 2011) (as distributed with MCNP6.2).

5 Variance reduction

In a typical NPP MCNP model described in this chapter, the magnitude of the total neutron flux in regions of interest ranges by more than 16 orders of magnitude. This, together with the presence of numerous neutron streaming paths, leads to an extremely difficult neutron transport problem, requiring humongous amounts of computational time. In order to obtain precise results within a reasonable amount of time, it is imperative to accelerate the calculations.

For a stochastic code like MCNP this can be accomplished by biasing the random walk of the tracked particles in a way to more frequently sample those histories, which most contribute to the targeted result (tally), all while maintaining the statistical validity (X-5 Monte Carlo Team 2008). This is referred to as *variance reduction* (VR).

5.1 Cell splitting

Historically, this has been accomplished using a technique called *cell-splitting*. It involves splitting the MCNP model geometry cells into a number of smaller cells, with importances (I) defined for each cell, such that they increase in the direction in which it's desirable for particles to move (e.g., through layers of shielding). When the tracked particle crosses the boundary between cell n and cell $n+1$, their relative importance is considered. If $\mathrm{I_{n+1}} > \mathrm{I_n}$ then the particle is split into $\frac{\mathrm{I_{n+1}}}{\mathrm{I_n}}$ particles, with their weight adjusted by $\frac{\mathrm{I_n}}{\mathrm{I_{n+1}}}$ (times the original weight). On the other hand, if $\mathrm{I_{n+1}} < \mathrm{I_n}$, then the tracked particle undergoes a Russian roulette, with a chance of survival of $\frac{\mathrm{I_{n+1}}}{\mathrm{I_n}}$. If it survives, its weight is increased by $\frac{\mathrm{I_n}}{\mathrm{I_{n+1}}}$. If it doesn't, its weight is set to zero and the particle is no longer tracked.

This technique has been employed extensively over the history of MCNP (X-5 Monte Carlo Team 2008, Pantelias Garcés 2013). Its application is generally intuitive (at least for cases with a single predominant transport direction of interest) and quantifiable – the user can track the success of applied importance set by looking at the number of particles in each cell (cell populations), which he ought to keep approximately constant. However, the use of this technique requires modification of the geometry, which increases the geometrical complexity of the model (with the number of cells often increasing by more than an order of magnitude) and potentially requires a lot of engineering time to implement these changes.

Given the already high level of complexity of the geometry in the NPP MCNP models developed as part of AMAC, as well as the large number of streaming pathways (rather than one dominant direction for the desirable neutron transfer), the usage of this particular variance reduction method is undesirable.

5.2 Weight-window generator (WWG)

In order to avoid the need to modify the geometry and in an effort to provide new features, the functionality of cell-splitting was later extended into a new technique – the *weight windows* (WW) (X-5 Monte Carlo Team 2008). Instead of splitting each cell into a number of smaller cells, the whole geometry is here overlaid with an independent, user-defined mesh structure. Each mesh cell is assigned a weight, which acts similarly to the cell importance described previously, except that the initiation of splitting or Russian roulette depends on the particle weight rather than the adjacent mesh cells. That is, each mesh cell has a bound of weights, with an upper and a lower bound. As such, splitting or Russian roulette only has to be performed when the particle weight

falls outside of the bounds, rather than at each cell boundary. With the dependence on cell boundaries gone, the technique also introduces energy dependence. That is, weight-windows are space-energy dependent.

Weight windows can be generated using a weight window generator (WWG) built into the MCNP (Liu & Gardner 1997). However, in order for the WWG to work, some tally response is required, as this response is used to calculate the importance of each (energy-space) mesh cell, depending on the (weight-weighted) fraction of the tally-scoring particles which have passed through this cell. This produces an importance map, which is then used to define the individual weight bounds.

Since tally response is required to produce a WW map, which is (for complex problems, at least) required to obtain a tally response, the user might encounter a causality dilemma type of situation, struggling to get those first tally scores. In these cases, some geometry modifications may be necessary – changing shielding density, for example. However, even after some tally response is achieved and the weight window map is generated, in general this first version is far from the optimum one. WW generation thus becomes an iterative process, in which the user must repeatedly use a WW map to generate a better WW map.

5.3 Hybrid variance reduction with ADVANTG

In an effort to address these limitations of WWG, ORNL has developed a hybrid variance reduction code ADVANTG (Automated Variance Reduction Generator) (Mosher et al. 2013). ADVANTG generates WW parameters based on a deterministic solution of the problem at hand.

In order to generate a WW map optimized for a single tally response, ADVANTG uses the CADIS (Consistent Adjoint-Driven Importance Sampling) method (Wagner & Haghighat 1998). A deterministic transport code is used to solve the adjoint of the neutron transport equation, with the solution interpreted as the "importance" of neutrons (at the particular location) to the optimized detector response. This allows the usage of the CADIS method to define the WW boundaries, with the weight boundaries inversely proportional to the adjoint flux.

However, a typical MCNP run tries to capture numerous quantities of interest, such as a single tally with multiple energy bins or multiple tallies. In this case, the FW-CADIS (Forward-weighted CADIS) method (Wagner et al. 2014) is used. In this method, first an adjoint source is constructed from all tallies of interest, weighted by the inverse of their individual responses. Afterwards, an additional calculation of the deterministic transport code is required, in order to solve the forward flux and estimate the aforementioned responses. This information is then used to define WW, which would lead to equal relative errors for all quantities of interest.

In order for ADVANTG to apply a deterministic solver (to solve the adjoint of the neutron transport equation), it must first translate the MCNP combinatorial geometry into a structured Cartesian grid compatible with the three-dimensional discrete ordinates transport solver Denovo (Evans et al. 2010). This is accomplished by the ray-tracing module of ADVANTG called LAVA, which defines the corresponding material mixtures for each mesh cell (Mosher et al. 2013). (Note that this is the same module, whose ray-tracing capability is used to define materials to be activated, as described in Chapter 6).

Once the Denovo problem is defined, the solution is obtained (either of just the adjoint flux, or both adjoint and forward flux), calculating the WW parameters for each Denovo cell. These are then printed out into a WW map file, in identical format as used by WWG.

The CADIS method also defines an approach for biased source distribution sampling, preferentially sampling regions of high importance. However, due to the limitations of the version of ADVANTG used (3.0), specifically the limited support for cell rejection, the source definition employed at Nagra is not compatible with the source biasing capability.

Motivated by the benefits ADVANTG has over the WWG and the cell-splitting variance reduction methods, it has been deployed at Nagra for the activation analysis problems since 2013 (Mosher et al. 2013, Pantelias Garcés 2013, Bykov 2014).

The version of the ADVANTG code suite presently used by AMAC is 3.2.0-nagra, developed by ORNL for Nagra. However, for the purposes of variance reduction, the functionality of this version is identical to version 3.2.0 distributed to the wider scientific community by RSICC and the NEA Data Bank (ORNL 2019a, ORNL 2019b).

6 Activation calculations

Neutron activation calculations, considering all the possible neutron-induced reactions and all elements present in each of the materials, are calculated using a separate code sequence. The information required to carry out activation calculations is summarized in Fig. 6-1 below. The calculations are approached component-wise – that is, the following activation sequence is repeated for each component.

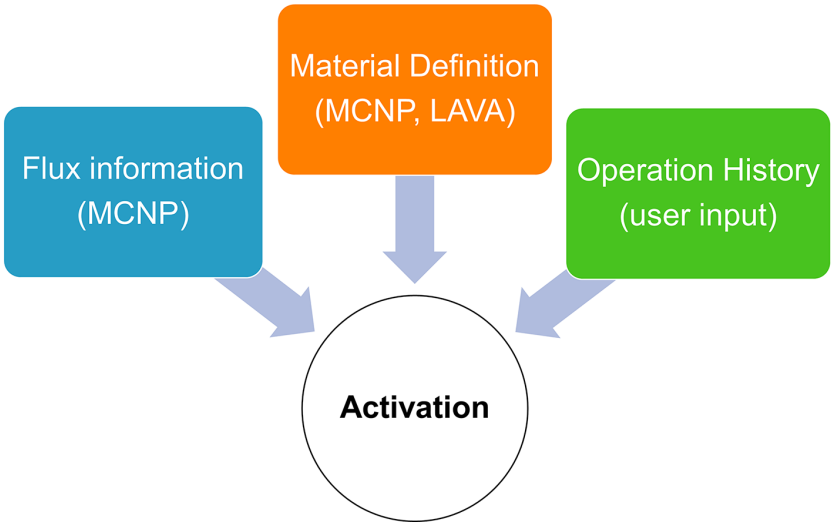

Fig. 6-1: Activation calculation inputs

The first step is to obtain a detailed description of the neutron flux distribution in the component using an MCNP calculation with a component-specific mesh tally. This is described in Chapter 4. A typical component would be described using 10^5–10^7 cells. This number determines the spatial resolution of the final activation characterization results. The energy distribution of the neutron flux in each cell is recorded at the resolution of 56 energy groups using the SCALE-56 energy group structure (Wieselquist et al. 2020).

The second step is the definition of materials to be activated. Specifically, the material inside each cell of the aforementioned mesh tally. This process is automated using the LAVA module, provided as part of the ADVANTG code (Mosher et al. 2013). The code loads the MCNP model into memory together with the mesh tally structure definition. These are then ray traced to determine the material content in each cell. The MCNP model used for this process is a modified version of the original MCNP model, where only the component surrounded by void is represented. That is, a separate input is prepared for each activated component. This assures that only the component material is activated and counted for the mass balancing. The output of the LAVA ray tracing procedure is the description of materials inside each cell of the mesh tally, thus providing the material definitions necessary for the activation calculations.

The final input for the activation calculations is the operating history. Since MCNP provides results normalized to the number of particles simulated, it is necessary to know the total neutron source strength. In addition to the neutron-induced activation reactions, it is also important to consider the radioactive decay taking place at the same time. All this information is provided by the NPP operating history, which defines the time-dependent source strength and (zero power) decay intervals. For the purpose of AMAC calculations for MIRAM-RBG, each cycle is

represented with one time step at the cycle-average power (and the corresponding neutron source strength) and one time step of zero power, corresponding to the subsequent outage. It should be noted, however, that this resolution represents a user choice, with the AMAC sequence supporting any number of power steps per cycle.

All these inputs – that is, flux information and material definition for each cell of the mesh tally, as well as the NPP operating history – are provided to the activation code ORIGEN. The communication between the codes used, as well as the handling of the user-provided data, is handled by the MSX code (distributed as part of the ADVANTG code suite (ORNL 2019a)).

MSX is in fact composed of several different codes. Firstly, msx_load loads the results of the MCNP mesh tally and the output of an ADVANTG calculation run to process the geometry with LAVA. The output of msx_load is a binary data file with all the aforementioned data. For cylindrical geometries, msx_load_rzt is used instead, initializing the LAVA calculation directly using a user provided MCNP geometry input file. Afterwards, msx_activate is used to load this binary data file and initialize a series of ORIGEN calculations – one for each mesh cell. For each cell of the mesh tally, ORIGEN solves a series of Bateman equations, computing the change of the material nuclide vector. This initialization is done through an API (application programming interface) built into ORIGEN (Wieselquist 2015), so no inputs or outputs are created. The ADVANTG suite includes a built-in version of ORIGEN, based on the SCALE 6.2 version of ORIGEN (Wieselquist et al. 2020). The operating history must be included as part of the msx_activate input file. Since this is a computationally intensive step, msx_activate is parallelized via the MPI (Message Passing Interface) protocol, so multiple ORIGEN calculations can be initialized simultaneously, reducing the overall (wall clock) time for the code execution. The output of msx_activate consists of number densities (number of nuclides per unit volume) of all present nuclides in each cell. In order to obtain other quantities of interest, the output data is post-processed by msx_post, which calculates cell mass and activities of all the nuclides. This module also offers the ability to visualize the results in a three-dimensional graphical format by outputting the calculated quantities in a binary format (as a SILO file) readable using the VisIt software (Bethel et al. 2012). This can be used to create pseudocolor graphics of specific activity distributions (or any other calculated quantities) in individual components or groups of components.

An example of such a plot can be seen in Fig. 6-2, showing the distribution of Co-60 specific activity (in Bq/g) within the KKM RPV and for reactor internals. The RPV including all reactor internals is shown on the left, and closeups of select reactor internals are shown on the right. Specifically, the steam dryer (top), the upper core plate (middle), and the fuel assembly feet (bottom). The same pseudocolor legend applies to all images.

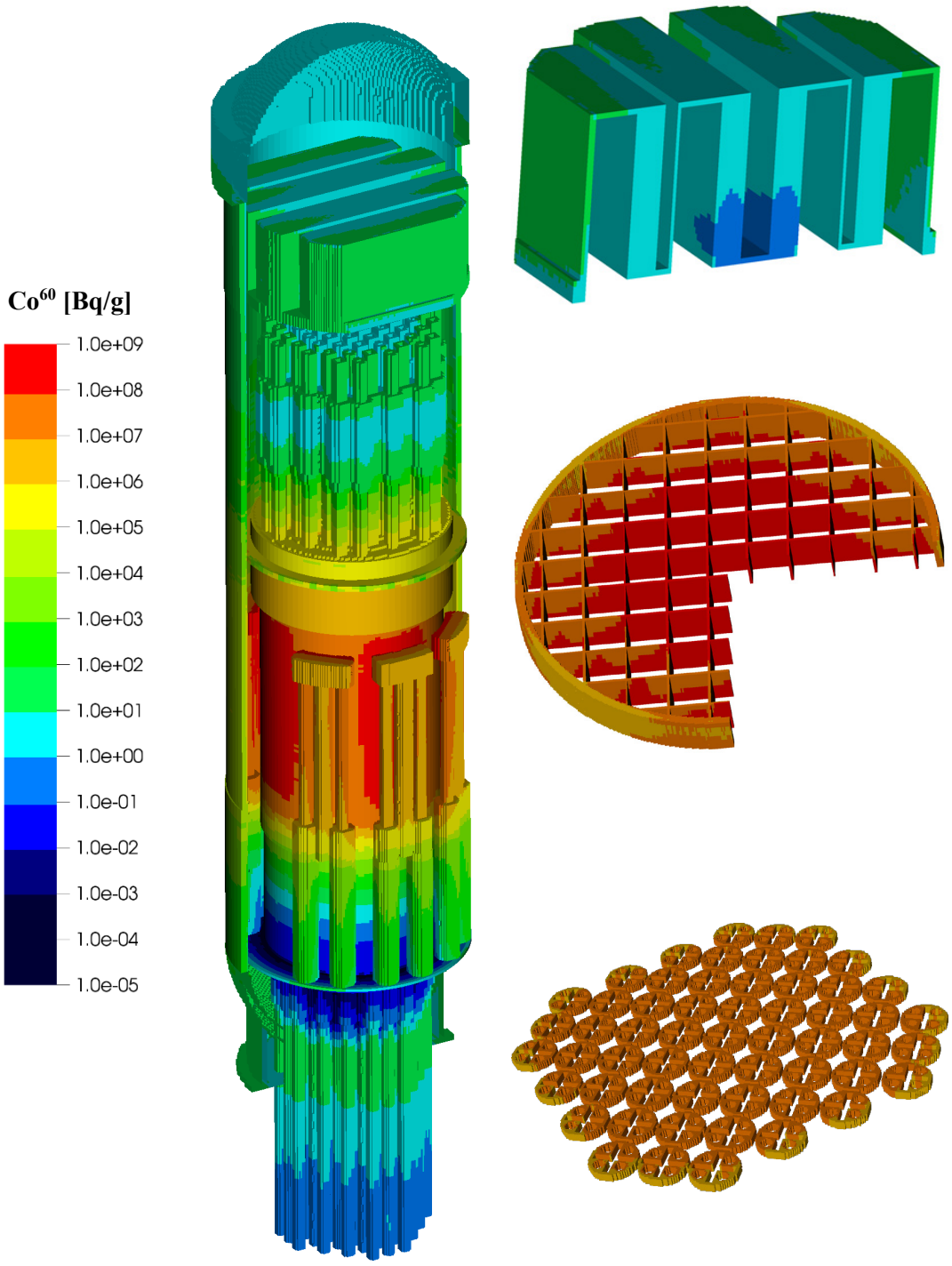

Fig. 6-2: Distribution of Co-60 specific activity in the KKM RPV and internals

Bykov (2019)

Left: RPV including reactor internals. Right: Closeups of three internal components: steam dryer (top), upper core plate (middle), and fuel assembly feet (bottom). Not to scale.

AMAC utilizes the ADVANTG code suite (ORNL 2019a) in code version 3.2.0-nagra, developed by ORNL for Nagra. This version is identical to the version 3.2.0 distributed to the wider scientific community by RSICC and the NEA Data Bank (ORNL 2019a, ORNL 2019b), except for the addition of extra post-processing capabilities to msx_post – most importantly, the ability to calculate the sum rule (as defined by StSV (StSV 2017)). The activation and decay calculations carried out by ORIGEN are also based on the ENDF/B-VII.1 library (Chadwick et al. 2011), as provided with the SCALE 6.2 release (Wieselquist et al. 2020).

When calculating the sum rule using this module, the calculation sequence simply uses the nuclide-specific clearance limits (LL), as defined in the StSV. However, some of these LL values already include the contribution from the daughter nuclides, which are then counted twice by the AMAC sequence. Since AMAC doesn't contain information about the origin of the daughter nuclides (e.g., there is no tracking of the presence of the parent nuclides), it is not possible to simply correct this. AMAC therefore (conservatively) overestimates the value of the sum rule in each cell. However, the nuclides affected by this have only a minor contribution to the total sum rule, which is typically dominated by key nuclides (such as Co-60 and Eu-152) which decay into stable daughters.

It should also be noted that this module calculates the sum rule based on the full nuclide inventory of the cell, including the naturally occurring radionuclides which were present in the base material before it was activated by neutrons. If this contribution is to be subtracted, the user needs to calculate the sum rule value of the base material (before any activation) and record it. This value should then be subtracted from all future sum rule evaluations. For example, if the natural concrete has a sum rule value of 0.82 (due to K-40, as well as the uranium and the thorium chains present in the impurities) and the user would like to check whether the activated material can be free released (i.e., has a sum rule value above 1.0), they should check whether the sum rule value is above 1.82, instead.

7 Validation

As with all simulations, validation is needed to build confidence in the results. Validation of AMAC calculations is typically done in two ways. The first approach, typically done when the power plant is still operating, validates the neutron flux using in-situ foil activation. The second approach, typically done following the final shutdown of the plant, validates the activity of the neutron activation induced radionuclides directly.

7.1 Flux validation

Flux validation is based on in-situ sample activation campaigns, in which thin metal foils of known mass and composition are placed, during a refueling outage, at key locations around the plant, such that they lie on the neutron streaming paths or in locations representative of an entire room. Fig. 7-1 shows a photograph from the placement of the activation foil at a key location in KKB. During the subsequent outage they are retrieved and analyzed with gamma spectrometry.

Fig. 7-1: Activation foils placed in KKB
Pisano (2018)

The validation foils are typically made up of cobalt, silver, scandium, and nickel. These foil materials predominately interact with neutrons at different (from each other) energies. Co-59, which undergoes an (n,γ) reaction, has an 836 b peak at 131 eV. Ag-109 undergoes an (n,γ) reaction with a 20500 b peak at 5.22 eV. Ni-58 undergoes an (n,p) reaction with a threshold of

approximately 500 keV and with the majority of reactions occurring at even higher energies. As such, Ni-58 activation is representative of the fast neutron flux. In later AMAC validation campaigns, additional foils made of Scandium were also added. The relevant cross sections (based on ENDF/B-VII.1), as well as the capsule holding the foils, are shown in Fig. 7-2.

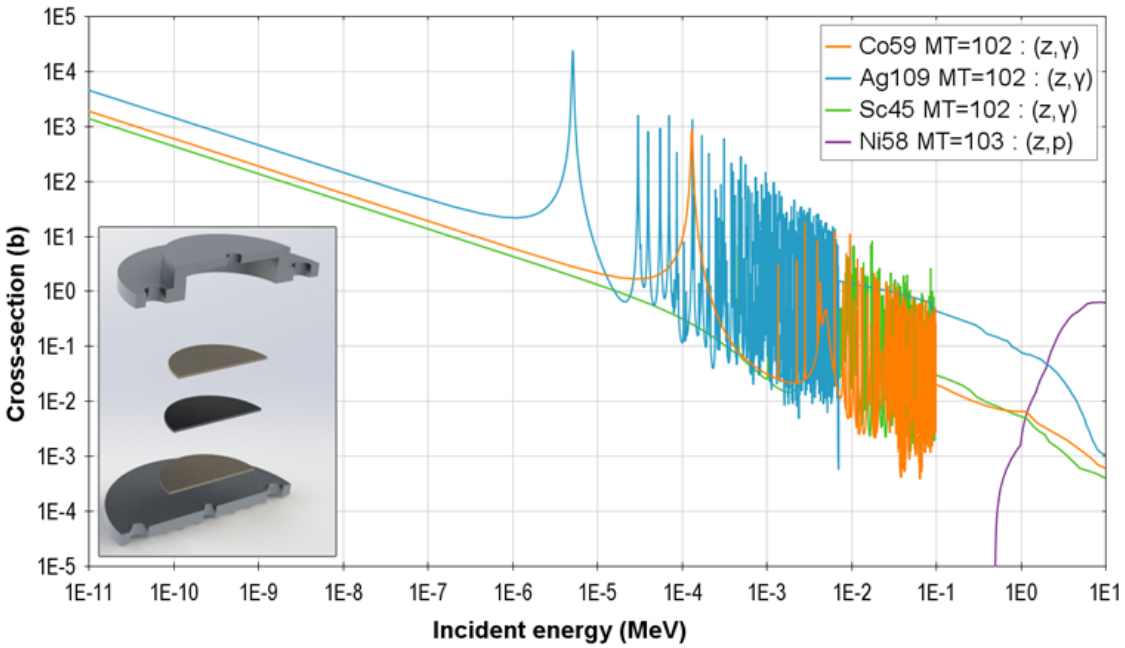

Fig. 7-2: Cross sections of relevant foil activation reactions

Bottom left: extruded cut view of a validation sample (variant with three foils inside a capsule).

The measured activity, corresponding to neutron-induced activation of the foil material, is also calculated using the MCNP model. The calculated and measured values are compared, with the agreement expressed using "C/M factors" – ratios of calculated to measured activity.

This allows the model designer to gain insight into the model sensitivity to variations in chosen parameters and modeling approaches, thus building an understanding of the key streaming pathways for each plant.

Once the validation comparison results are available, they are used to steer the updates of the MCNP model. That is, areas in which the C/M factors are much larger than the target level of agreement (as defined in Section 7.3) are revisited, and all supporting documentation is re-evaluated with the aim of explaining the larger-than-expected deviations. These may be caused by missing or superfluous streaming paths – both associated with insufficient level of model detail – as well as through the presence of undocumented material (e.g., insulation), or wrong dimensions. That is, causes which affect the neutron transport towards or away from the area in question. The postulated explanations for the differences are tested against the existing technical drawings and discussed with the NPP staff familiar with the area in question.

7.2 Direct sampling

The second technique used for the validation of AMAC models is based on the (mainly gamma, but sometimes also alpha and beta) spectrometry of the actual activated materials. In general, this can only be performed after the final shutdown of the analyzed installation, when the removal of material (such as bioshield concrete) doesn't affect safety. Alternatively, this analysis can be performed during the replacement (or removal) of components, or on not safety relevant materials (e.g., concrete wall which doesn't have any radiation shielding function).

The activation distribution of reactor internals – which are the most activated and thus the most important components for the packaging concept and the MIRAM-RBG nuclide inventory database – cannot be fully validated before the final shutdown. Limited point-wise validation may be possible in case of internal component replacements.

This type of validation of AMAC-calculated activities was for example carried out during the decommissioning of the Basel research reactor. Fig. 7-3 shows a drill core resulting from drilling into the floor of the reactor pool. As can be seen from the individual layers, the drill core first passed through the bottom of the (aluminum) tank, as well as araldite and bitumen layers, before finally reaching the concrete. Each layer was then analyzed with gamma spectrometry. The concrete part of the drill core was further split into axial segments, with each analyzed separately. This provided information about the depth dependence of the nuclide activities.

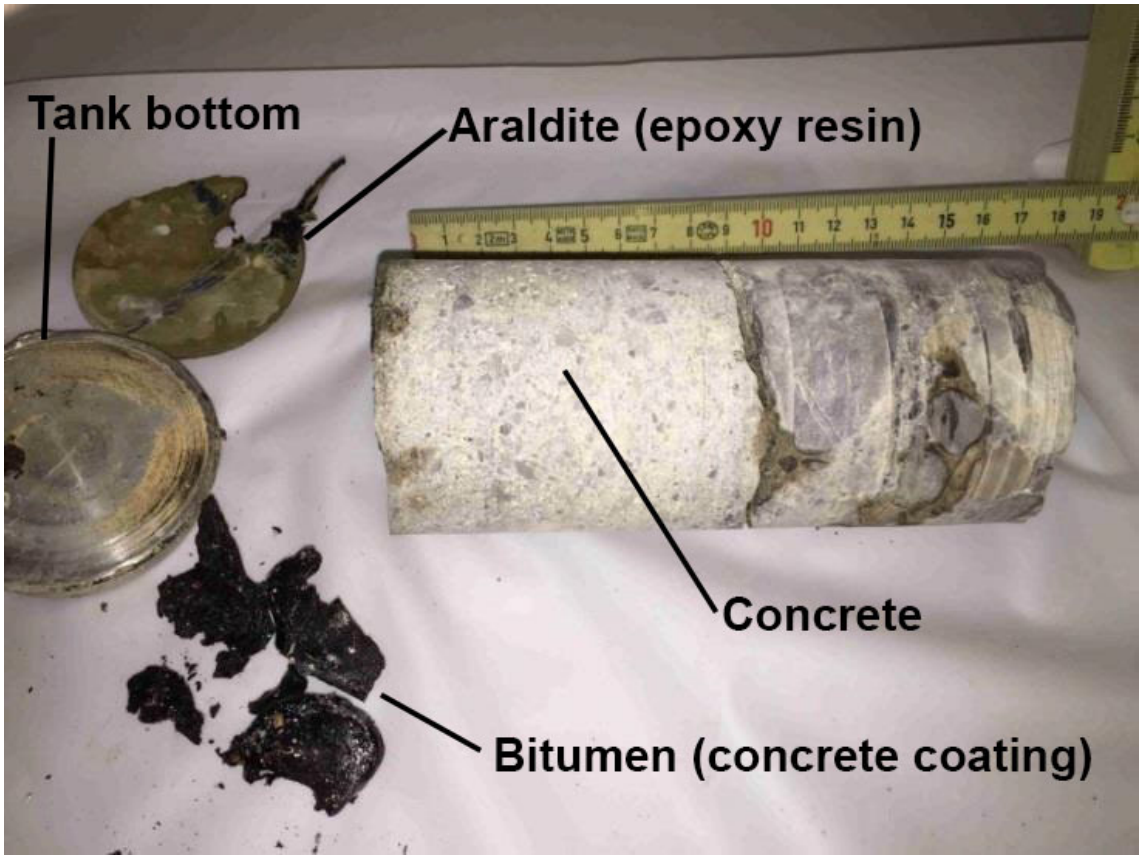

Fig. 7-3: Drill core extracted from the Basel research reactor
Bykov (2019)

As can be seen from this example, the sample extraction procedure is similar to the procedure for obtaining samples for material analysis, described in Chapter 2. Specifically, the drill core shown in Fig. 7-3 is similar to the drill core shown in Fig. 2-1. The difference is only in the subsequent analysis performed on the sample.

7.3 Target level of accuracy

The target accuracy is based on the expected impact of the activity overestimation on the subsequent applications of these results.

Most of the core internals are highly activated. When considering the application of AMAC to decommissioning planning, as described in Chapter 9, the exact activity of these components determines the necessary shielding of the waste casks into which these components will be packaged. Therefore, a significant overestimation of the activity of these components will lead to overestimated shielding requirements, and therefore sub-optimal packing strategies and increased costs. This overestimation would also have a significant impact on the total nuclide inventory of the decommissioning waste –the key quantity for MIRAM and the subsequent safety analyses.

On the other hand, the structures located further away from the core (such as the drywell in KKM) are only slightly activated. In this case the output of interest is the total volume of waste (i.e., the quantity of material above clearance limits) – this is described in Chapter 10. Given that the neutron flux inside concrete drops very quickly with depth, even a significant overestimation (e.g., C/M of 3) results in an only marginal increase in activation depth and therefore total waste volume. As such, the decommissioning planning actions are less sensitive to the flux overestimation in these areas. The low activity also means that these components don't significantly contribute to the overall decommissioning waste nuclide vector inventory (which is dominated by the highly activated reactor internals).

In accordance with this philosophy, the following C/M values are targeted:

- C/M between 1.0 and 1.5 for regions inside and in the immediate vicinity of the RPV
- C/M between 1.5 and 2.0 for regions further away from the core (such as the top of the bioshield or the reactor pit area below PWR RPVs)
- C/M between 2.0 and 3.0 for the even further away areas (such as the BWR drywell or the pool area above PWR RPV head)

These target factors are also inherently linked to the systematic overestimation resulting from the empty room assumption. The further particles travel through these rooms, the higher the cumulative flux overestimation will be. For this reason, it's impossible to achieve a low C/M in these areas, without compensating for the (shielding-wise not-modeled) empty rooms.

8 AMAC Data Tools

The activation calculations described in Chapter 6 produce a large amount of data, with each component described via $10^5 – 10^7$ cells, each with a full nuclide vector. In order to support the organization, storage, and analysis of this data, data management (AMAC-Database, AMAC-DatabaseUtilities) and data analytics (AMAC-Dashboard, AMAC-Notebooks) tools have been developed. Together, these software tools are denoted as AMAC Data Tools.

All python packages (which together comprise the AMAC Data Tools) are stored and developed in a private GitHub (GitHub, Inc.) repository, which assures version control, but also provides tools for access control and an environment for tracking bugs and feature requests.

8.1 AMAC-Database

AMAC-Database is a database solution developed for collecting and organizing the activation results (output by the MSX code). It is written in the Python programming language (VanRossum & Drake 2010) and leverages the HDF5 technology (HDF Group 1997) for data storage. Processed activation results are stored in one or multiple HDF5 files (Database files). There is always one Database file for each power plant.

The AMAC Database file is an HDF5 file (filename extension .h5). HDF5 is a binary file format with an inner hierarchical structure of Groups and Datasets. It can be thought of the HDF5 file as a file system within a file. In this imaginary file system, Groups represent *folders* while Datasets represent *files*. Each Database file contains all of the obtained activation results (for all components at all calculated timestamps), material information, and information about the NPP (including the operation history used for the calculations, as well as various metadata).

8.2 AMAC-DatabaseUtilities

AMAC-DatabaseUtilities is a Python package simplifying retrieval of data from the Database files and their analysis. The package is also used for building and managing Database files and is required for a full functionality of the AMAC-Database package.

The AMAC-DatabaseUtilities package consists of two main sub-packages: dbutils and ALGOPACK. Dbutils is a collection of Python modules serving various purposes such as building Database files or retrieving and plotting AMAC data. ALGOPACK is an algorithm developed to evaluate the optimal strategy for the segmentation and packaging of NPP activation waste. It is described in more detail in Section 8.3.

The AMAC-DatabaseUtilities package comes with a suite of (hundreds of) automated tests that can be used to validate proper functionality of the package.

8.3 ALGOPACK

ALGOPACK (Algorithm-optimized packaging) is the second of the two main sub-packages of AMAC-DatabaseUtilities. It is a package developed to evaluate the optimal strategy for the segmentation and packaging of strongly activated NPP components.

When provided with a component activity distribution, ALGOPACK determines the packaging concept which minimizes the total container costs (within the defined boundary conditions and waste container specifications).

This problem corresponds to the general description of a two-dimensional vector bin packing problem with variable bin sizes. Following this description, the packing problem is first formulated in mathematical notation. This can then be solved using existing solution algorithms. However, compared to the generic cases, the segmentation and packing optimization problem at hand has some unique constraints. Specifically, it is assumed that the component will be segmented along a single direction (e.g., from top to bottom), with the removed segment (after any further cutting, as required) being immediately placed inside the selected container before removing the next segment. It is also expected that a container will have to be fully filled (and closed) before another container can be selected, leading to a continuous sequential packaging.

The core challenge solved by ALGOPACK is the identification of the most preferential container, performed at the beginning of the segmentation process and following each closure of a full container. To identify the ideal container, dynamic programming is used to evaluate for each available container type the corresponding most-efficient packing (given the segments next in line to be packaged), as constrained by volume and activity limits. That one container is then selected, which contains the highest ratio of waste mass to container cost (while satisfying all constraints, including the container-specific generic packing densities and hotspot factor limits[1]).

The algorithm loads each cask with sequential component segments (corresponding to cells output by AMAC activation sequence), checking against various limit criteria (such as the activity limit and the available inner packaging volume).

ALGOPACK is based on several abstractions (types of objects):

- Waste Item, representing components or their parts. They are three-dimensional.
- Waste Segment, the zero-dimensional slices of Waste Items. They are created through the process of segmentation – by slicing the Waste Item along the segmentation axis in the segmentation direction.
- Container is a representation of a physical waste disposal container such as LC-84 or MOSAIK-II. Containers store Waste Segments.
- Packing Problem defines the optimization task and facilitates its execution.
- Packing Solution stores results (the solution) of the Packing Problem and provides methods for result validation and further processing (e.g., calculation of averaged Container properties per container type).

The ALGOPACK optimization algorithm is a sequential packing algorithm with an assumption of continuous segmentation and packaging. It is composed of the following steps:

1. First, a list of Waste Items is defined. This includes selecting the segmentation axis and segmentation direction for each Waste Item.
2. Next, the Packing Problem is created for the list of Waste Items, a list of available container types, and a table of container parameters.
3. Then, the *PackingProblem.solve()* method is called. Its logic is shown in Fig. 8-1.
4. The Packing Problem solver performs the segmentation of Waste Items into Waste Segments.

---

[1] The hotspot factor limit is defined as a limit on the maximum ratio of the highest specific activity (from all the segments loaded into the given waste container) to the container-average specific activity. This accounts for cases with strongly heterogeneous activity distribution, where the total activity loaded into the container is acceptable, but a concentration of activity leads to a dose rate hotspot.

5. Selection of the best combination of containers is performed sequentially.
6. The process first creates a batch of empty containers (one of each available type).
7. All container types are simultaneously filled by sequential placement of Waste Segments.
8. Once any of the containers is full, it is marked as such, and the list of all leftover Waste Segments (those segments which are not yet placed into a container) is remembered.
9. Once all containers from the current batch are full, the best container from the batch is chosen by maximizing the ratio: stored waste mass / container cost.
10. The leftover Waste Segments of the best container type are then packaged again with a new batch of empty container types.
11. This process is repeated until all Waste Segments are placed into containers.

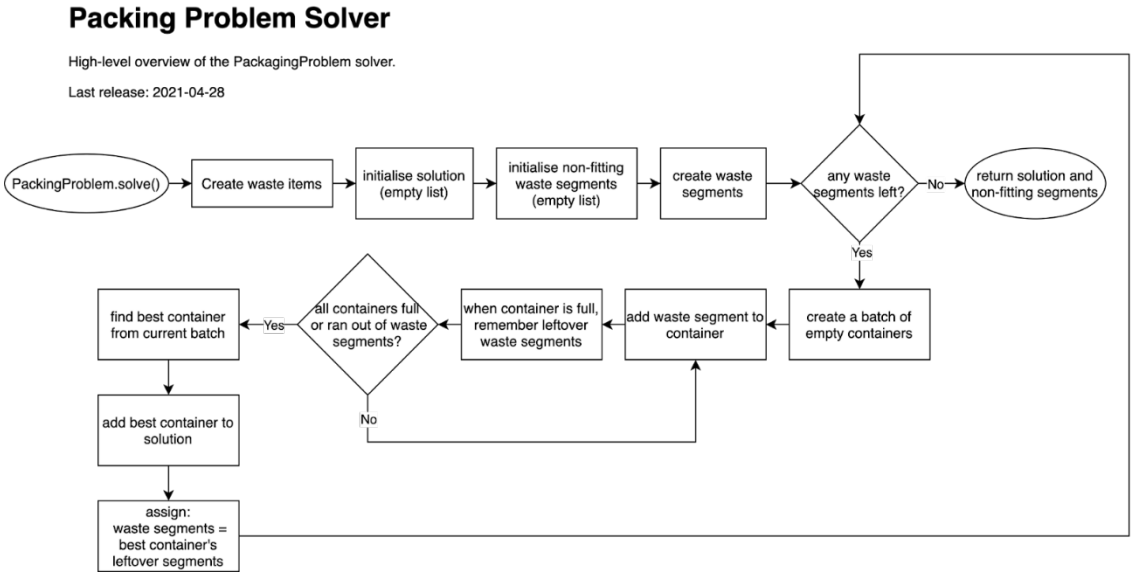

Fig. 8-1: PackingProblem solver high-level (low detail) flow chart

The limit criteria are applied on the containers to determine whether or not the current waste content (list of Waste Segments) fits into the container. The considered limit criteria are:

- activity limit: the total activity of selected nuclides against the maximum activities allowed by their respective (e.g., transport) license applications or otherwise assumed in the boundary conditions
- hot-spot factor limit, enforcing that the local specific activity cannot be much higher than the homogeneously distributed specific activity assumed in the studies that defined the Activity limit
- mass limit: the maximum total mass of a loaded container (including the mortar filling, if applicable), as limited by the assumed container stacks
- volume limit: the available inner volume of each waste container, as limited by the assumed maximum fill fraction
- minimum loading limit: the minimum allowed loading of each container

8.4 AMAC-Dashboard

AMAC-Dashboard is a web application created for presentation and analysis of activation results in a user-friendly way. A screenshot of the user interface can be seen in Fig. 8-2. This application runs on a central server, access to which is provided to authorized users, who can then access it through a web browser. The website they access consists of several sub-sites:

- component catalog for simple access to the activation results, which the user can browse for individual components by specifying the combination of NPP, Component, and Timestamp
- packaging concepts: the integration of ALGOPACK and AMAC-Dashboard. The site allows for execution of ALGOPACK packaging tasks and for presentation of the results
- balancing Tool, which allows to quickly compare multiple components against each other
- documentation: the full user and administrator manual to AMAC Data Tools

Overall, AMAC-Dashboard aims to provide easy-to-use analysis tools for the most common analysis requests. However, its functionality is limited to the tools explicitly programmed into the web application.

8.5 AMAC-Notebooks

For more complicated requests and analysis that goes beyond the functionality built into the AMAC-Dashboard, AMAC-Notebooks were created. AMAC-Notebooks is an instance of JupyterHub (Project Jupyter) equipped with AMAC-DatabaseUtilities and with access to AMAC Database files. Similarly to the AMAC-Dashboard, the authorized users can access this server via their web browsers. The accessed page provides a computational environment for creating and managing so-called notebook documents – virtual environments for literate programming. No configuration is necessary from the users, as this is performed on the server side.

Through AMAC-Notebooks, the users have access to all of the data in all of the available AMAC Database files, which they can retrieve and post-process using tools from the AMAC-DatabaseUtilities package, or any other tools from any Python library. This makes AMAC-Notebooks extremely versatile and capable of performing virtually any kind of data analysis on the activation results.

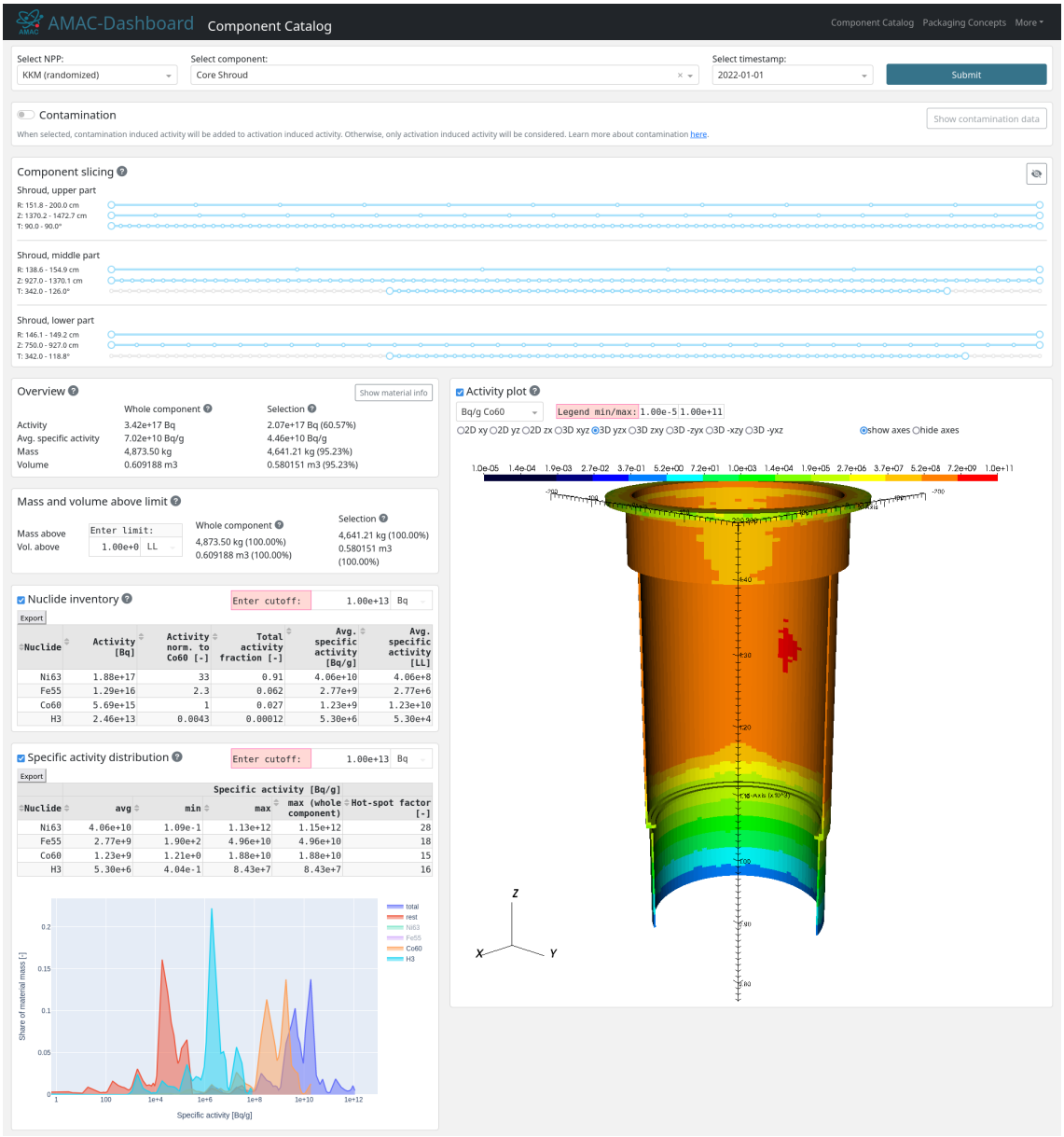

Fig. 8-2: Screenshot of AMAC-Dashboard (showing test data)

9 Packaging concept optimization

The knowledge of the activity distribution in each component is used to select an appropriate waste container. However, for components with a significant activity gradient, this selection is non-trivial, as different sections of the component could be best suited for different types of waste containers. As such, there is a lot of optimization potential in defining the set of waste containers to be used for these components. For this purpose, a program named ALGOPACK was created. Its functionality is described in Section 8.3.

For all decommissioning waste, the number of waste packages calculated for KS21 is preserved for MIRAM-RBG. As such, the KS21 approaches for the development of packaging concepts, including all boundary conditions, are also carried forward to the present work.

The packaging concept for KKG and KKL was developed by Nagra on the basis of ALGOPACK optimization calculations. For these two NPPs, the MIRAM-RBG approach was to reproduce the ALGOPACK calculations carried out for KS21 and use the newly developed AMAC Data Tools modules to reconstruct the full nuclide inventory of each AGT using the full nuclide vectors stored in the AMAC Database files.

The waste containers considered for the ALGOPACK calculations are: GNS MOSAIK-II (Gesellschaft für Nuklear-Service (GNS) mbH 2019) with various thicknesses of inner lead shielding, LC-84, LC-84-Plus, and LC-86 concrete containers. All container-specific limits (following the KS21 boundary conditions) are provided to ALGOPACK.

The packaging concepts for KKM and KKB were developed directly by the NPP staff on the basis of past Nagra activation calculations. That is, these concepts are not based on ALGOPACK optimization calculations and don't necessarily follow the same constraints. As such, an alternative approach had to be defined to estimate the nuclide vectors for all of the AGTs associated with the components included in the NPP-internal packaging concept. It should be noted that even in these custom packaging concepts, it was known which component was packaged into which type of waste container. Only in cases where a single component was packed into multiple types of waste containers, the division of the total component nuclide vector between the AGTs needed to be determined. This was done by assuming that the segmentation of components into the different waste container types follows the division of their overall Co-60 activity. That is, for all nuclides, the fraction of the total component activity packed into a given AGT is given as a ratio of Co-60 activity in the corresponding waste package and the total Co-60 activity in the component. While this is only a rough approximation, as the spatial distribution of many nuclides differs from the spatial distribution of Co-60 (as governed by the shape of the relevant cross sections), it is deemed sufficient for the target purpose of MIRAM-RBG (long term safety analysis). It should be noted that the overall, whole component nuclide vector is conserved – this approach merely approximates how it is divided.

For MIRAM-RBG, the application of ALGOPACK and the subsequent definition of the AGT-specific nuclide vectors is done in the AMAC-Notebooks environment (as described in Section 8.5). Specifically, for each NPP, a notebook is created, in which the relevant data is retrieved from the corresponding AMAC Database file and then post-processed following the methodology described in this chapter. The notebooks also include code for exporting the nuclide vectors for each relevant AGT. That is, these notebooks will allow future users to reproduce all of the work done and obtain the exact data that is provided for MIRAM-RBG.

10 Analysis of the surrounding structures

The surrounding structures – that is, all structures outside of the RPV, including the bioshield, the drywell, as well as the content and walls of any distant rooms – typically have very low activities. StSV (StSV 2017) provides a number of mechanisms for dealing with such low-activity material. Following the boundary conditions of KS21, MIRAM-RBG considers free release, decay storage, and disposal in deep geological repository. For some sections of these components the activities are so low that they are deemed not dangerous to the general public and can be released from regulatory control. That is, when the activity is lower than the clearance limits, the so-called free release is possible. Decay storage refers to the deferment of the release of the material from regulatory control. That is, material is kept in a storage facility for up to 30 years with the goal to free release it after this period. Finally, when the activity is too high for either of these mechanisms, the material is disposed of in the deep geological repository, together with the RPV and reactor internals.

Some surrounding structures are assumed to be disposed of completely, without any consideration of free release or decay storage – even if the AMAC results would suggest that parts of the components *would* be eligible for these other disposal methods. This is often motivated by the high difficulty of carving out the parts with lower activity, and the overall low amount of material that would benefit from this sorting. An example of this is the KKM bioshield. For these components, the waste volume is simply equal to the full component volume, and the associated nuclide vector corresponds to the total component nuclide vector divided by the number of waste containers used for its packaging.

However, for most surrounding structures, it is first necessary to select the relevant sections of the component, destined for the deep geological disposal. This is done by querying the component data from the AMAC Database file and applying a *mask* to the component. For example, in order to create the selection mask for the KKM drywell concrete, the corresponding data is queried at the time point of 36 years after shutdown (that is, following 30 years of decay storage). The sum rule is calculated in each cell and cells where the sum rule is higher than 1.0 (with the contribution of naturally occurring radionuclides subtracted as described in Chapter 6) at this time point. These cells represent the sections, which will still be not eligible for free release after 30 years of decay storage and are therefore (per KS21 boundary conditions) assigned to the deep geological disposal. This selection of cells is saved as a mask, which is then applied to both concrete and reinforcement steel at the time point of 6 years after shutdown (that is, before any decay storage). That is, segments which would not benefit from decay storage are already disposed now, without being sent to decay storage.

Note that the same mask is applied to the concrete and its reinforcement steel materials. As explained in Chapter 6, concrete and rebar steel are activated separately. They each occupy the total volume (i.e., they always completely overlap), but fill it only with their partial density. Per KS21 boundary conditions, no separation of rebar from concrete is assumed to take place. That is, each segment of reinforced concrete where either concrete *or* the reinforcement steel are not eligible for free release must be treated as radioactive waste.

Since MIRAM-RBG seeks parity with KS21 for the number of waste packages, any scaling of the neutron fluxes or individual nuclide activities (based on results of validation as described in Chapter 7) that was assumed for KS21 is also applied for this work. However, this is done on a case-by-case basis and its documentation is therefore beyond the scope of this report.

Once the mask is used to select the relevant parts of the component, the nuclide vector of the selection is simply divided by the number of waste containers, producing the container-averaged nuclide vectors for MIRAM-RBG. This is possible because all components are always packaged into a single type of waste container, and therefore only have a single AGT assigned to them.

The definition of the mask, and its application to the activation data from the AMAC Database files, is done in the AMAC-Notebooks environment (as described in Section 8.5). Specifically, for each NPP, a notebook is created, in which the relevant data is retrieved from the corresponding AMAC Database file and then post-processed following the methodology described in this chapter. The notebooks also include code for exporting the nuclide vectors for each relevant AGT. That is, these notebooks will allow future users to reproduce all of the work done and obtain the exact data that is provided for MIRAM-RBG.

11 References

Bethel, E.W., Childs, H. & Hansen, C. (2012): High Performance Visualization. Chapman and Hall/CRC

Bykov, V. (2014): Enhancement and validation of the NPP Mühleberg MCNP activation simulations for Swiss decommissioning planning MSc Thesis. ETH Zürich

Bykov, V. (2019): High-Fidelity Determination of Nuclide Inventories for Radioactive Waste Disposal

Chadwick, M.B., Herman, M., Obložinský, P., Dunn, M.E., Danon, Y., Kahler, A.C., Smith, D.L., Pritychenko, B., Arbanas, G., Arcilla, R., Brewer, R., Brown, D.A., Capote, R., Carlson, A.D., Cho, Y.S., Derrien, H., Guber, K., Hale, G.M., Hoblit, S., Holloway, S., Johnson, T.D., Kawano, T., Kiedrowski, B.C., Kim, H., Kunieda, S., Larson, N.M., Leal, L., Lestone, J.P., Little, R.C., McCutchan, E.A., MacFarlane, R.E., MacInnes, M., Mattoon, C.M., McKnight, R.D., Mughabghab, S.F., Nobre, G., Palmiotti, G., Palumbo, A., Pigni, M.T., Pronyaev, V.G., Sayer, R.O., Sonzogni, A.A., Summers, N.C., Talou, P., Thompson, I.J., Trkov, A., Vogt, R.L., van der Marck, S.C., Wallner, A., White, M.C., Wiarda, D. & Young, P.G. (2011): ENDF/B-VII.1 Nuclear Data for Science and Technology: Cross Sections, Covariances, Fission Product Yields and Decay Data. Nuclear Data Sheets 112/12, 2887-2996. DOI: 10.1016/j.nds.2011.11.002

DIN (2013): Classification of shielding concretes by proportion of elements - Part 1: Neutron shielding

Evans, J.C., Lepel, E.L., Sanders, R.W., Wilkerson, C.L., Silker, W., Thomas, C.W., Abel, K.H. & Robertson, D.R. (1984): Long-lived activation products in reactor materials

Evans, T.M., Stafford, A.S., Slaybaugh, R.N. & Clarno, K.T. (2010): Denovo: A New Three-Dimensional Parallel Discrete Ordinates Code in SCALE. Nuclear Technology 171/2, 171-200. DOI: 10.13182/nt171-171

Gesellschaft für Nuklear-Service (GNS) mbH (2019): MOSAIK® Transport- und Lagerbehälter für MAW, available online at https://www.gns.de/language=de/21620/mosaik, status as of 19.9.202

GitHub, Inc. (2022): GitHub, available online at https://github.com/, Stand am 19. September 2022

HDF Group (1997): Hierarchical Data Format, version 5, available online at https://www.hdfgroup.org/HDF5/, Stand am 19. September 2022

Liu, L. & Gardner, R.P. (1997): A Geometry-Independent Fine-Mesh-Based Monte Carlo Importance Generator. Nuclear Science and Engineering 125/2, 188-195. DOI: 10.13182/nse97-a24265

McConn, R.J., Gesh, C.J., Pagh, R.T., Rucker, R.A. & Williams III, R. (2011): Compendium of Material Composition Data for Radiation Transport Modeling

Mosher, S.W., Bevill, A.M., Johnson, S.R., Ibrahim, A.M., Daily, C.R., Evans, T.M., Wagner, J.C., Johnson, J.O. & Grobe, R.E. (2013): ADVANTG – An Automated Variance Reduction Parameter Generator. (ORNL/TM-2013/416). Oak Ridge National Laboratory, available online at https://info.ornl.gov/sites/publications/Files/Pub46035.pdf, status as of 29.10.2021

Nagra (2014): Modellhaftes Inventar für radioaktive Materialien – MIRAM 14. Nagra Technischer Bericht NTB 14-04

Nagra (2023): Modellhaftes Inventar für radioaktive Materialien MIRAM-RBG. Nagra Technischer Bericht NTB 22-05

ORNL (2019a): CCC-854 - ADVANTG 3.2.0: AutomateD VAriaNce reducTion Generator with ORNL-TN. Version 3.2.0. RSICC, available online at https://rsicc.ornl.gov/codes/ccc/ccc8/ccc-854.html, Stand am 19. September 2022

ORNL (2019b): CCC-854 - ADVANTG 3.2.0: AutomateD VAriaNce reducTion Generator with ORNL-TN. Version 3.2.1. NEA Data Bank, available online at https://www.oecd-nea.org/tools/abstract/detail/ccc-0854/, Stand am 19. September 2022

Pantelias Garcés, M. (2013): Activation Neutronics for the Swiss Nuclear Power Plants. Diss. ETH. No 21623. ETH, Zürich

Pisano, P.G. (2018): Application and validation of the Nagra activation calculation methodology to the Beznau NPP and development of a packaging concept for RPV and internals. Master Thesis. École Polytechnique Fédérale de Lausanne EPFL

Project Jupyter (2022): JupyterHub, available online at https://jupyter.org/hub, Stand am 19. September 2022

Scolaro, A. (2016): Implementation of the Nagra activation calculation methodology for the Gundremmingen Nuclear Power Plant. Master Thesis. École Polytechnique Fédérale de Lausanne EPFL, available online at https://www.researchgate.net/publication/322569887_Implementation_of_the_Nagra_Activation_Calculation_Methodology_for_the_Gundremmingen_Nuclear_Power_Plant

StSV (2017): Strahlenschutzverordnung (StSV) vom 26. April 2017, Stand am 1. Januar 2022. Systematische Sammlung des Bundesrechts SR 814.501, Schweiz

Tamaseviciute, E. (2011): Neutron Streaming Investigation outside the RPV of the Gösgen Nuclear Power Plant with the Monte Carlo Method MSc Thesis. ETH Zürich

VanRossum, G. & Drake, F. L. (2010): The Python language reference. Release 3.0.1 [repr.]. Python documentation manual, / Guido van Rossum; Fred L. Drake [ed.] ; Pt. 2, [Hampton, NH], [Redwood City, Calif.]. Python Software Foundation; SoHo Books

Volmert, B. & Pantelias Garcés, M. (2011a): Stilllegungsstudie 2011: Radiologische Inventare der aktivierten Grundmaterialien des KKB. Nagra Arbeitsbericht NAB 11-13

Volmert, B. & Pantelias Garcés, M. (2011b): Stilllegungsstudie 2011: Radiologische Inventare der aktivierten Grundmaterialien des KKG. Nagra Arbeitsbericht NAB 11-14.

Volmert, B. & Pantelias Garcés, M. (2011c): Stilllegungsstudie 2011: Radiologische Inventare der aktivierten Grundmaterialien des KKL. Nagra Arbeitsbericht NAB 11-11

Volmert, B. & Pantelias Garcés, M. (2011d): Stilllegungsstudie 2011: Radiologische Inventare der aktivierten Grundmaterialien des KKM. Nagra Arbeitsbericht NAB 11-12

Wagner, J.C. & Haghighat, A. (1998): Automated Variance Reduction of Monte Carlo Shielding Calculations Using the Discrete Ordinates Adjoint Function. Nuclear Science and Engineering 128/2, 186-208. DOI: 10.13182/nse98-2

Wagner, J.C., Peplow, D.E. & Mosher, S.W. (2014): FW-CADIS Method for Global and Regional Variance Reduction of Monte Carlo Radiation Transport Calculations. Nuclear Science and Engineering 176/1, 37-57. DOI: 10.13182/nse12-33

Werner, C. J. (ed.) (2017): MCNP User's Manual - Code Version 6.2. Rev. 0. (LA-UR-17-29981). Los Alamos National Laboratory, available online at https://mcnp.lanl.gov/pdf_files/la-ur-17-29981.pdf, status as of 19.09.2022

Wieselquist, W. A., Lefebvre, R. A. & Jessee, M. A. (ed.) (2020): SCALE Code System. Version 6.2.4. (ORNL/TM-2005/39). Oak Ridge National Laboratory

Wieselquist, W.A. (2015): The SCALE 6.2 ORIGEN API for High Performance Depletion. *In:* Proceedings of the M&C 2015 Conference

X-5 Monte Carlo Team (2008): MCNP - A General N-Particle Transport Code, Version 5. (LA-UR-10-06235). Los Alamos National Laboratory, available online at https://mcnp.lanl.gov/pdf_files/la-ur-03-1987.pdf, status as of 19.09.2022